# Type I band alignment in $GaAs_{81}Sb_{19}$/GaAs core-shell nanowires

T. Xu,[1,2] M. J. Wei,[2] P. Capiod,[1] A. Díaz Álvarez,[1] X. L. Han,[1] D. Troadec,[1] J. P. Nys,[1] M. Berthe,[1] I. Lefebvre,[1] G. Patriarche,[3] S. R. Plissard,[1,4] P. Caroff,[1,5] Ph. Ebert,[6] and B. Grandidier[1,a)]

[1]*Institut d'Electronique, de Microélectronique et de Nanotechnologies (IEMN), CNRS, UMR 8520, Département ISEN, 41 bd Vauban, 59046 Lille Cedex, France*
[2]*Key Laboratory of Advanced Display and System Application, Shanghai University, 149 Yanchang Road, Shanghai 200072, People's Republic of China*
[3]*CNRS-Laboratoire de Photonique et de Nanostructures (LPN), Route de Nozay, 91460 Marcoussis, France*
[4]*CNRS-Laboratoire d'Analyse et d'Architecture des Systèmes (LAAS), Univ. de Toulouse, 7 Avenue du Colonel Roche, F-31400 Toulouse, France*
[5]*Department of Electronic Materials Engineering, Research School of Physics and Engineering, The Australian National University, Canberra, Australian Capital Territory 0200, Australia*
[6]*Peter Grünberg Institut, Forschungszentrum Jülich GmbH, 52425 Jülich, Germany*

(Received 10 July 2015; accepted 2 September 2015; published online 15 September 2015)

The composition and band gap of the shell that formed during the growth of axial GaAs/$GaAs_{81}Sb_{19}$/GaAs heterostructure nanowires have been investigated by transmission electron microscopy combined with energy dispersion spectroscopy, scanning tunneling spectroscopy, and density functional theory calculations. On the $GaAs_{81}Sb_{19}$ intermediate segment, the shell is found to be free of Sb (pure GaAs shell) and transparent to the tunneling electrons, despite the (110) biaxial strain that affects its band gap. As a result, a direct measurement of the core band gap allows the quantitative determination of the band offset between the $GaAs_{81}Sb_{19}$ core and the GaAs shell and identifies it as a type I band alignment. © *2015 AIP Publishing LLC*. [http://dx.doi.org/10.1063/1.4930991]

Narrow band gap antimonide-based III-V semiconductors are promising materials for the fabrication of photonic and electronic devices with high tunability and enhanced performances.[1,2] They can cover a wide infrared wavelength range and allow great flexibility in engineering different types of band alignment as well as refractive index. This is particularly the case for the $GaAs_{1-x}Sb_x$ system, that has been used as the active layer of infrared lasers.[3,4] While the two-dimensional growth of such a ternary compound has proven to suffer from low miscibility,[5] compositional broadening at the interfaces,[6] and misfit dislocations,[7] high quality material has been recently obtained in the nanowire (NW) form.[8–11] Indeed, axial heterostructure NWs are known to sustain higher lattice mismatch, due to a more efficient lateral strain relaxation.[12–14]

However, the growth of axial heterostructure NWs is not solely axial but usually involves radial growth, i.e., the deposition of materials on the sidewall facets.[15–18] Such a small lateral overgrowth by a thin layer of GaAs is expected during the growth of axial $GaAs_{1-x}Sb_x$/GaAs heterostructure NWs. Recently, it was even found that the Sb content on the periphery of $GaAs_{1-x}Sb_x$ segments is reduced, due to an enhanced exchange of Sb atoms by As atoms at the surface of the NWs,[19] suggesting the existence of a pure GaAs shell around the $GaAs_{1-x}Sb_x$ segment. Because the lattice parameters of zinc blende (ZB) $GaAs_{1-x}Sb_x$ and GaAs are different, strain should affect the bang gap of the GaAs shell, due to the interplay between the bond strength in crystals and the band structure.[20] Such an effect has been advantageously used in optoelectronics to extend the wavelength range in optical emission and absorption spectra of semiconductor heterostructures.[21,22] Questions thus arise regarding the contribution of the GaAs shell to the electrostatic potential profile and band offsets along the NW radial direction in order to tailor the confinement of the charge carriers in axial $GaAs_{1-x}Sb_x$ /GaAs heterostructure NWs.

In this work, we investigate axial $GaAs_{81}Sb_{19}$/GaAs heterostructure NWs that have been grown by molecular beam epitaxy. Analysis of the Sb distribution across the $GaAs_{81}Sb_{19}$ segment by means of transmission electron microscopy (TEM) combined with energy-dispersive X-ray spectroscopy (EDX) reveals the existence of a thin shell around the $GaAs_{81}Sb_{19}$ segment. Although this shell is essentially free of Sb atoms at the surface, scanning tunneling spectroscopy (STS) indicates an apparent band gap that is much smaller than the band gap of pure GaAs. *Ab-initio* calculations of the evolution of GaAs band gap under (110) biaxial strain are unable to account for the band gap narrowing. Conversely, the measured band gap fits well with the band gap of a $GaAs_{81}Sb_{19}$ alloy, demonstrating a type I heterostructure with a shell thin enough to leave that barrier transparent to tunneling electrons.

The growth of the axial heterostructure NWs was achieved with Ga seed particles using the vapor-liquid-solid mechanism, as described previously.[23,24] The NW structure shown in Fig. 1(a) consists of a ZB GaAs bottom segment, a ZB $GaAs_{1-x}Sb_x$ intermediate segment with a nominal Sb concentration $x$ of 0.19 (labelled $GaAs_{81}Sb_{19}$), and a GaAs top segment with intended lengths of 800 nm, 400 nm, and 400 nm, respectively. $GaAs_{1-x}Sb_x$ NWs with a nominal composition $x$ of 0.5 were also grown with the same growth conditions (labelled $GaAs_{0.5}Sb_{0.5}$) and used as reference samples for STS measurements. At the end of the growth, all the NWs were capped with a thin As layer, deposited at

a)E-mail: bruno.grandidier@isen.iemn.univ-lille1.fr

 © 2015 AIP Publishing LLC

This article is copyrighted as indicated in the article. Reuse of AIP content is subject to the terms at: http://scitation.aip.org/termsconditions. Downloaded to IP: 140.93.5.25 On: Tue, 15 Sep 2015 14:04:54

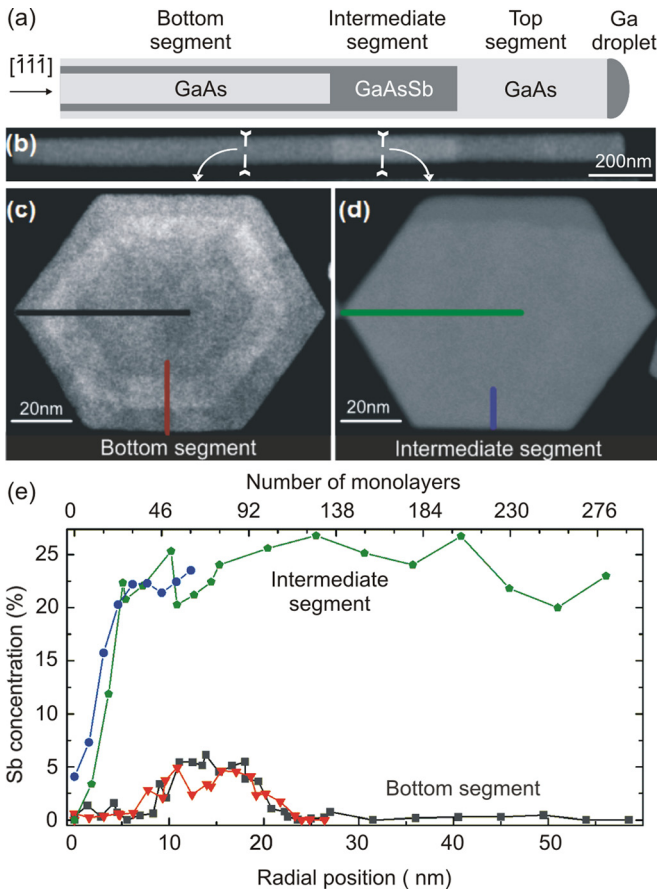


FIG. 1. (a) Schematic of the GaAs/GaAsSb heterostructure nanowire. (b) HAADF STEM image of GaAs/$GaAs_{0.81}Sb_{0.19}$ nanowire heterostructure. (c) HAADF STEM cross-sectional view of the bottom segment. (d) HAADF STEM cross-sectional view of the intermediate segment. (e) Sb concentration profile deduced from EDX point scan analyses performed along the colored segments defined in the cross-sectional views. The origins of the radial profiles start at the NW sidewall.

room temperature for 50 min under high $As_4$ flux to protect the NWs from air exposure (oxidation).[17]

The NWs were first analysed using TEM. For that purpose, the NWs were transferred onto a silicon substrate with a good control over the orientation of the NWs.[25] Then, they were buried under a 120 nm-thick layer of hydrogen silsesquioxane (HSQ) and thin slices, perpendicular to the NW main axis, were extracted using a focused ion beam. Scanning transmission electron microscopy (STEM) was performed on an aberration-corrected microscope (Jeol 2200FS) with EDX capacity. The EDX point analyses used a probe size of about 1 nm and a probe current of about 150 pA (half-convergence of 30 mrad). The NWs were also characterized by low-temperature (77 K) scanning tunneling microscopy (STM) in ultrahigh vacuum, after the complete desorption of the As capping layer and the subsequent cleavage of the NWs onto a silver terminated Si(111) substrate.[17]

Figure 1(b) shows a typical high angle annular dark field (HAADF) STEM micrograph of two axial GaAs/$GaAs_{81}Sb_{19}$/GaAs heterostructure NWs. The $GaAs_{81}Sb_{19}$ segment is identified from its bright contrast with respect to the GaAs segments. Its position as well as its length are consistent with the intended structure of the NWs. From high resolution TEM images (not shown), interface abruptnesses of 4.5 +/− 0.5 and 17.0 +/− 0.5 nm were, respectively, found for the GaAs bottom segment/GaAsSb and GaAsSb/GaAs top segment interfaces. The cross-sectional HAADF-STEM view of the bottom segment in Fig. 1(c) shows a hexagonal shape with the existence of a double shell, indicating radial overgrowth each time a new segment is grown along the main axis of the NW. This observation suggests the existence of a shell around the $GaAs_{81}Sb_{19}$ segment. The shell is however not resolved in Fig. 1(d), but detected in the quantitative EDX analysis shown below. Note that the dark contrast seen parallel with the top sidewall of the hexagonal cross-section in Fig. 1(d) is an artefact from the sample preparation.

Quantitative concentration profiles extracted from the EDX analyses are displayed in Fig. 1(e). In the bottom segment, the profile of the Sb content is consistent with the contrast variations visible in the HAADF-STEM image. It outlines the existence of a hexagonally shaped $GaAs_{1-x}Sb_x$ quantum well with $x = 0.04 \pm 0.02$, that is surrounded by two GaAs potential barriers. In the intermediate segment, the profile of the Sb content indicates a $GaAs_{81}Sb_{19}$ core with a slightly higher Sb content than the nominal one. Remarkably, the Sb concentration is reduced close to the sidewalls, and this drop is even more acute at the vertices of the NWs. As seven NWs were investigated in this way and all showed the same profile, such a result demonstrates the existence of a few nm thin Sb-poor shell around the $GaAs_{81}Sb_{19}$ segment, in agreement with Ref. 19.

In order to corroborate the absence of Sb at the surface of the $GaAs_{81}Sb_{19}$ segment, the sidewalls were imaged with STM.[17] The $GaAs_{81}Sb_{19}$ segment can be identified from its bright contrast in the STM image of Fig. 2(a). This contrast, corresponding to a topographic change of 2–3 nm, indicates a slight difference in diameter. The difference in diameters for these two sections is attributed mainly to a change of the wetting configuration/volume of the droplet during growth of the GaAsSb segment[26] and also to a lattice relaxation. The sidewall of the $GaAs_{81}Sb_{19}$ segment is atomically flat and sprinkled with single atomic layer terraces that have nucleated at the border of the sidewalls. High resolution STM images obtained on the sidewall, such as the one seen in Fig. 2(b), exhibit the atomic sublattice of a ZB {110} face, without significant contrast variation between the atoms. This observation differs from the corrugation seen on the sidewall of a ZB GaAsSb NW with 50% Sb nominal composition (see Fig. 2(d)), where numerous bright protrusions, typical of antimony atoms are clearly resolved.[17] Therefore, the STM characterization of the sidewalls supports the formation of a Sb-free shell around the $GaAs_{81}Sb_{19}$ segment of the heterostructure NWs.

Tunneling spectroscopic measurements were further performed to determine the electronic structure of the shell. Spectrum (i) of Fig. 3 obtained on the pure ZB GaAs segment, far from the interface, shows a width of the voltage region without current that is in agreement with the band gap of ZB GaAs (~1.50 eV). Similarly, spectrum (iii) obtained on the ZB GaAsSb NW reveals a smaller band gap of 0.75 eV, which is close to the theoretical band gap of $GaAs_{50}Sb_{50}$.[5,27] Finally, spectrum (ii), measured in the center of the $GaAs_{81}Sb_{19}$ segment, yields a band gap of 1.1 eV, that is between the band gap of GaAs and $GaAs_{50}Sb_{50}$. As

This article is copyrighted as indicated in the article. Reuse of AIP content is subject to the terms at: http://scitation.aip.org/termsconditions. Downloaded to IP: 140.93.5.25 On: Tue, 15 Sep 2015 14:04:54

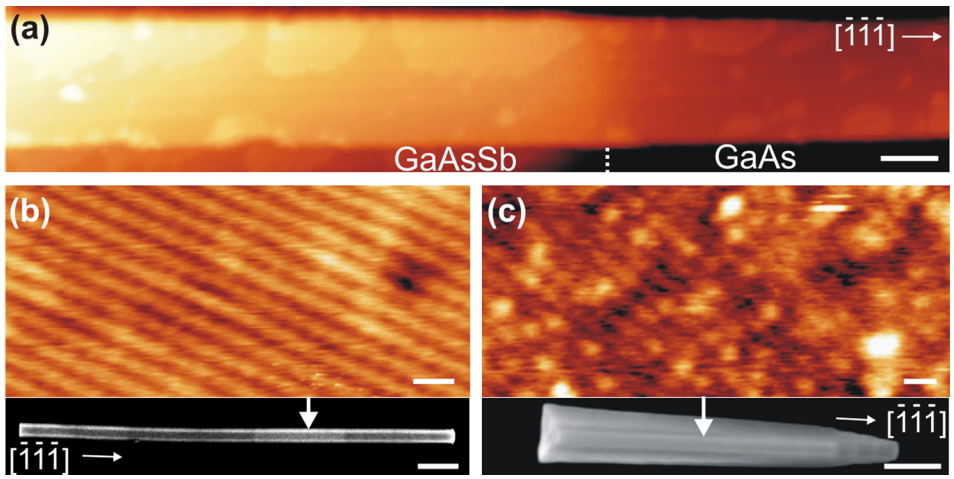


FIG. 2. (a) STM image of the interface between the intermediate segment and the top segment of a GaAs/$GaAs_{81}Sb_{19}$ NW sidewall. Experimental parameters: tunneling current of 10 pA, sample voltage of +2.8 V, and temperature of 77 K. Scale bar: 25 nm. (b) and (c) High resolution occupied state STM images obtained on the {110} sidewall of the intermediate segment of the heterostructure NW and on the {110} sidewall of the $GaAs_{50}Sb_{50}$ NW, respectively. Experimental parameters: tunneling current of 100/20 pA, sample voltage of −2.0 V/−3.5 V, and temperature of 77 K. Scale bar: 0.4 nm. Insets: SEM images of a GaAs/$GaAs_{81}Sb_{19}$/GaAs NW and a $GaAs_{50}Sb_{50}$ NW, respectively. Scale bars: 200 nm. The arrows point at the position where the STM images have been acquired.

the shell is almost pure GaAs (strong Sb depletion, see above), the effect of the strain on the band gap of a GaAs shell was investigated first. A thin GaAs shell is expected to be tensile (110) biaxial strained when grown on a $GaAs_{81}Sb_{19}$ substrate. For that purpose, we studied the evolution of the GaAs band gap as a function of the in-plane strain by means of electronic structure computations, in the Density Functional Theory (DFT) Framework. All total energy calculations were performed with the Vienna *ab initio* simulation program [VASP, version 5.2.11],[28] using all electron projector augmented wave (PAW) pseudopotentials,[29] with the Ceperley and Alder approximation,[30] parameterized by Perdew and Zunger for exchange and correlation energies (i.e., the As, Ga_d, H1.25 and H.75 PAW potentials). To account for the band splittings, we included spin-orbit (SO) coupling explicitly in the calculations. All calculations were done using a kinetic energy cutoff of 456.28 eV. The lattice constant of the GaAs unit cell was calculated to be 5.6102 Å, in good agreement with an experimental value of 5.6533 Å (the relative discrepancy is about 0.77%).

We first considered a bulk-like GaAs unit cell corresponding to GaAs(110) under the biaxial strain due to growth on the $GaAs_{1-x}Sb_x$. The in-plane $a_x$ parameter has been estimated by mean of a Vegard's law (relative to the optimized GaAs parameter). The $c_x/a_x$ parameter was optimized for different Sb content (see Table I). To take into account the (110) surface, supercells containing six GaAs layers were constructed with the lower surface of the slab saturated by H atoms and the two first layers fixed to the bulk-like optimized positions. The six layer-thick slabs were separated by a vacuum region equivalent to a distance of seven layers which has been demonstrated to be sufficient.[31] All structures were optimized with respect to the ionic positions, using a quasi-Newton-method for relaxation, until the forces on all atoms were less than 1 meV/Å. A (3 × 3 × 1) Monkhorst-Pack *k*-point grid was used for the relaxation of surface structures. The local density of states was computed on the supercells in order to discriminate surface from "bulk-like" contributions. The tetrahedron method with Blöchl corrections was used to determine how the partial occupancies are set. Computations were done on a (10 × 10) Monkhorst-Pack *k*-point meshes of the surface Brillouin zone.

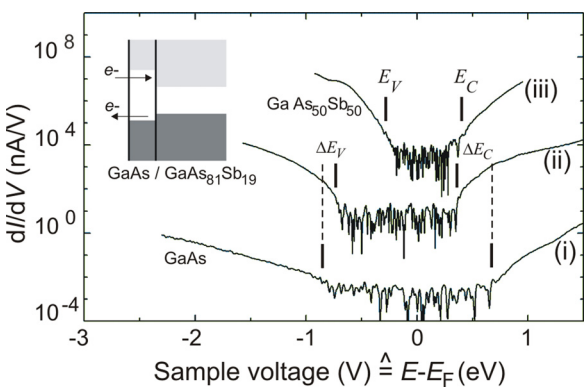


FIG. 3. Tunneling spectra acquired on (i) the pure GaAs top segment and (ii) the shell surrounding the $GaAs_{81}Sb_{19}$ segment of a GaAs/$GaAs_{81}Sb_{19}$/GaAs heterostructure NW, as well as (iii) a $GaAs_{50}Sb_{50}$ NW. All spectra were acquired at 77 K with tunneling conditions of (i) 1.6 V, 0.8 nA, (ii) 1.6 V, 0.8 nA, and (iii) −1.0 V, 0.5 nA. Spectra (ii) and (iii) have been shifted for clarity. The conduction $E_C$ and valence $E_V$ band edges are indicated by vertical segments, while $\Delta E_C$ and $\Delta E_V$ correspond to the band offsets between GaAs and the $GaAs_{81}Sb_{19}$ core. Inset: Energy band diagram of the radial GaAs/$GaAs_{81}Sb_{19}$ heterostructure, the arrows indicating the tunneling of electrons from or into the $GaAs_{81}Sb_{19}$ core through the GaAs shell.

TABLE I. Lattice parameters and in-plane strain as a function of the Sb content.

| Sb content | $a_x$ | Optimized $c_x$ | In-plane strain |
|---|---|---|---|
| 0 | 5.6102 | 3.9670 | 0 |
| 0.2 | 5.6987 | 3.9470 | 0.0158 |
| 0.4 | 5.7872 | 3.9323 | 0.0316 |
| 0.8 | 5.9643 | 3.8900 | 0.0631 |

This article is copyrighted as indicated in the article. Reuse of AIP content is subject to the terms at: http://scitation.aip.org/termsconditions. Downloaded to IP: 140.93.5.25 On: Tue, 15 Sep 2015 14:04:54

Figure 4 summarizes the evolution of the bulk and surface band gap for strained GaAs(110): the band gap decreases with strain. Previous calculations for biaxially strained GaAs(001) and (111) corroborate this trend.[32,33] However, such a decrease is clearly not enough when the biaxial strain is caused by a core corresponding to a Sb content $x$ of ~0.2 only. Therefore, strain is unable to account for the measured band gap narrowing.

In contrast, if we consider unstrained $GaAs_{1-x}Sb_x$ material, the evolution of the measured band gap as a function of the Sb content fits well with the theoretical band gap calculated from the linear interpolation between the parameters of GaAs and GaSb according to the Vegard's law[5] drawn as a solid line in Fig. 4. This indicates that tunneling spectroscopy reveals the band edge position of the $GaAs_{81}Sb_{19}$ core in the intermediate segment. The shell acts as a potential barrier and is transparent to the tunneling electrons transferred in the energy range corresponding to the shell band gap. This is consistent with the observed shell thickness of a few nanometers only, as deduced from the compositional analysis of the core-shell NWs in cross-section. Hence, the radial band alignment between the GaAs shell and the $GaAs_{81}Sb_{19}$ core is of type I as indicated by the inset in Fig. 3. The values of the band offsets can be determined from the spectra on the pure GaAs and the $GaAs_{81}Sb_{19}$ segments: The top surface is in both cases GaAs with the Fermi energy pinned by extrinsic midgap surface states arising from steps.[24] Their energy position is essentially unaffected by a quantum confinement in the thin GaAs shell and can serve as reference energy. Therefore, the valence ($\Delta E_V$) and conduction ($\Delta E_C$) band offsets are directly measured in Fig. 3 to be 0.1 and 0.3 eV, respectively.

In conclusion, axial $GaAs_{81}Sb_{19}$/GaAs heterostructure NWs grown by molecular beam epitaxy are found to exhibit a thin pure GaAs shell around the core. This shell is transparent to tunneling electrons allowing the direct determination of the nature of the band alignment between the $GaAs_{81}Sb_{19}$ core and the GaAs shell of the NWs. Due to the lack of intrinsic surfaces states on the (110) surfaces of most III–V semiconductor materials, we expect tunneling spectroscopic experiments to be relevant to a large variety of other core-shell nanowires grown along a ⟨111⟩ direction in order to gain insight into the band discontinuities of those heterostructures.

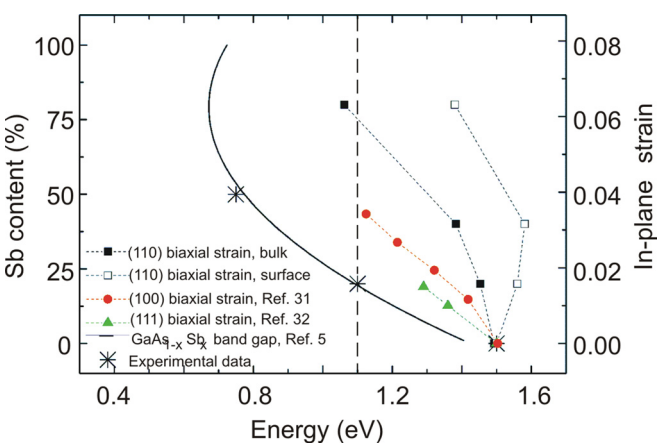


FIG. 4. Evolution of the band gap of differently oriented biaxially strained GaAs layers as a function of the in-plane strain, right axis (or in terms of the Sb content for $GaAs_{1-x}Sb_x$, left axis). The vertical dashed line indicates the experimental value of the band gap measured on the shell. The calculated data for pure unstrained GaAs are shifted to match the experimental bulk band gap. Similarly, the calculated surface band gap is matched to the measured one of about 1.5 eV.[24]

This study was financially supported by the European Community's Seventh Framework Program (Grant No. PITN-GA-2012-316751, "Nanoembrace" Project), the EQUIPEX program Excelsior, the RENATECH network, and the Impuls- und Vernetzungsfonds of the Helmholtz-Gemeinschaft Deutscher Forschungszentren (Grant No. HIRG-0014). T. Xu acknowledges the support of the Region Nord-Pas-de-Calais and of the National Natural Science Foundation of China (Grant No. 61204014). The authors thank X. Wallart for fruitful discussions.

[1]B. R. Bennett, R. Magno, J. B. Boos, W. Kruppa, and M. G. Ancona, Solid-State Electron. **49**, 1875 (2005).
[2]C. Liu, Y. Li, and Y. Zeng, Engineering **2**, 617 (2010).
[3]F. Quochi, D. C. Kilper, J. E. Cunningham, M. Dinu, and J. Shah, IEEE Photonics Technol. Lett. **13**, 921 (2001).
[4]E. Gesrter, I. Ecker, S. Lorch, C. Hahn, S. Menzel, and P. Unger, J. Appl. Phys. **94**, 7397 (2003).
[5]R. E. Nahory, M. A. Pollack, J. C. DeWinter, and K. M. Williams, J. Appl. Phys. **48**, 1607 (1977).
[6]R. Kaspi and K. R. Evans, J. Cryst. Growth **175/176**, 838 (1997).
[7]T. Wosińki, A. Makosa, T. Figielski, and J. Raczyńka, Appl. Phys. Lett. **67**, 1131 (1995).
[8]D. L. Dheeraj, G. Patriarche, L. Largeau, H. L. Zhou, A. T. J. van Helvoort, F. Glas, J. C. Harmand, B. O. Fimland, and H. Weman, Nanotechnology **19**, 275605 (2008).
[9]D. L. Dheeraj, G. Patriarche, H. L. Zhou, T. B. Hoang, A. F. Moses, S. Gronsberg, A. T. J. Van Helvoort, B. O. Fimland, and H. Weman, Nano Lett. **8**, 4459 (2008).
[10]S. Plissard, K. A. Dick, X. Wallart, and P. Caroff, Appl. Phys. Lett. **96**, 121901 (2010).
[11]X. Yuan, P. Caroff, J. Wong-Leung, H. H. Tan, and C. Jagadish, Nanoscale **7**, 4995 (2015).
[12]F. Glas, Phys. Rev. **74**, 121302 (2006).
[13]M. W. Larsson, J. B. Wagner, M. Wallin, P. Håkansson, L. E. Fröberg, L. Samuelson, and L. R. Wallenberg, Nanotechnology **18**, 015504 (2007).
[14]M. de la Mata, C. Magén, P. Caroff, and J. Arbiol, Nano Lett. **14**, 6614 (2014).
[15]M. A. Verheijen, G. Immink, T. de Smet, M. T. Borgström, and E. P. A. M. Bakkers, J. Am. Chem. Soc. **128**, 1353 (2006).
[16]P. K. Mohseni, C. Maunders, G. A. Botton, and R. R. LaPierre, Nanotechnology **18**, 445304 (2007).
[17]T. Xu, K. A. Dick, S. Plissard, T. H. Nguyen, Y. Makoudi, M. Berthe, J.-P. Nys, X. Wallart, B. Grandidier, and P. Caroff, Nanotechnology **23**, 095702 (2012).
[18]J. V. Knutsson, S. Lehmann, M. Hjort, P. Reinke, E. Lundgren, K. A. Dick, R. Timm, and A. Mikkelsen, ACS Appl. Mater. Interfaces **7**, 5748 (2015).
[19]H. Kauto, B. O. Fimland, T. Grieb, A. M. Munshi, K. Müller, A. Rosenauer, and A. T. J. Van Helvoort, J. Appl. Phys. **116**, 144303 (2014).
[20]F. H. Pollak and M. Cardona, Phys. Rev. **172**, 816 (1968).
[21]K. Ozasa, M. Yuri, S. Tanaka, and H. Matsunami, J. Appl. Phys. **68**, 107 (1990).
[22]A. M. Smith, A. M. Mohs, and S. Nie, Nat. Nanotechnol. **4**, 56 (2009).
[23]C. Colombo, D. Spirkoska, M. Frimmer, G. Abstreiter, and A. Fontcuberta i Morral, Phys. Rev. B **77**, 155326 (2008).
[24]P. Capiod, T. Xu, J. P. Nys, M. Berthe, G. Patriarche, L. Lymperakis, J. Neugebauer, P. Caroff, R. E. Dunin-Borkowski, Ph. Ebert, and B. Grandidier, Appl. Phys. Lett. **103**, 122104 (2013).
[25]T. Xu, J.-P. Nys, A. Addad, O. I. Lebedev, A. Urbieta, B. Salhi, M. Berthe, B. Grandidier, and D. Stiévenard, Phys. Rev. B **81**, 115403 (2010).

This article is copyrighted as indicated in the article. Reuse of AIP content is subject to the terms at: http://scitation.aip.org/termsconditions. Downloaded to IP: 140.93.5.25 On: Tue, 15 Sep 2015 14:04:54

[26]S. R. Plissard, D. R. Slapak, M. A. Verheijen, M. Hocevar, G. W. G. Immink, I. van Weperen, S. Nadj-Perge, S. M. Frolov, L. P. Kouwenhoven, and E. P. A. M. Bakkers, Nano Lett. **12**, 1794 (2012).
[27]K. Alberi, J. Wu, W. Walukiewicz, K. M. Yu, O. D. Dubon, S. P. Watkins, X. Liu, Y.-J. Cho, and J. Furdyna, Phys. Rev. B **75**, 045203 (2007).
[28]G. Kresse and J. Furthmüller, Phys. Rev. B **54**, 11169 (1996).
[29]P. E. Blöchl, Phys. Rev. B **50**, 17953 (1994).
[30]D. M. Ceperley and B. J. Alder, Phys. Rev. Lett. **45**, 566 (1980).
[31]Ph. Ebert, B. Engels, P. Richard, K. Schroeder, S. Blügel, C. Domke, M. Heinrich, and K. Urban, Phys. Rev. Lett. **77**, 2997 (1996).
[32]P. R. C. Kent, G. L W. Hart, and A. Zunger, Appl. Phys. Lett. **81**, 4377 (2002).
[33]E. S. Kadantsev, M. Zieliński, and P. Hawrylak, Phys. Rev. B **86**, 085411 (2012).

This article is copyrighted as indicated in the article. Reuse of AIP content is subject to the terms at: http://scitation.aip.org/termsconditions. Downloaded to IP: 140.93.5.25
On: Tue, 15 Sep 2015 14:04:54